Equivalence between general acoustic Willis media and conventional materials with embedded sources

Mehmet Utku Demir [*] and Bogdan-Ioan Popa [†]
Department of Mechanical Engineering, University of Michigan, Ann Arbor, Michigan 48109, USA

Willis materials provide degrees of freedom to control mechanical waves unavailable in conventional materials, but our understanding of wave-matter interaction in these exotic media has been limited by their unconventional constitutive equations. This work derives an equivalence between the acoustic Willis wave equation inside a general inhomogeneous and anisotropic Willis medium and the well-known wave equation in conventional acoustic materials with embedded continuous distributions of monopole and dipole sources. It thus enables accurate and efficient computation of sound scattering from arbitrarily shaped general acoustic Willis materials in one, two, and three dimensions. The result is validated by showing in numerical simulations that realizable bulk Willis metamaterials, obtained by periodically replicating a labyrinthine cell, scatter sound identically to its equivalent material with embedded continuous source distributions. Furthermore, the equivalence provides insights into the physics of Willis materials. For example, it shows that multiple pairs of Willis coupling vectors produce exactly the same sound scattering regardless of excitation. It also directly shows whether the effective material parameters extracted from single Willis cell simulations maintain validity in bulk metamaterials based on that cell. This equivalence model will advance the design of Willis metamaterials and provide the tool to better understand the physics of Willis media.

Introduction. Willis media have long been recognized as extensions to conventional materials in which additional coupling coefficients between the strain-momentum and velocity-stress fields provide new degrees of freedom to manipulate sound [1–4]. Although Willis coupling is typically small in the natural acoustic environment, various studies have demonstrated that Willis coupling can be increased using metamaterial techniques which enabled exciting applications. For example, it has been shown that metasurfaces composed of arrangements of carefully designed unit cells significantly increase the Willis coupling coefficients and allow independent control of the reflected and transmitted sound [5]. Similarly, gradient Willis metasurfaces have been used as highly efficient beam steerers in which transmitted waves were sent in desired directions with very low reflections [6] and grating Willis metasurfaces have been used as anomalous reflectors that steered the reflected sound in nonspecular directions [7]. Moreover, a design approach based on self-induced surface waves was introduced and experimentally verified to realize Willis gradient metasurfaces for arbitrary beam splitting and anomalous reflection with theoretically unitary efficiency [8].

Active Willis metamaterials further extended the range of achievable Willis coupling coefficients beyond the fundamental limitations of passive media. Not only that the two Willis coefficients can be set differently in active media, but their values are not subject to the fundamental bounds imposed in passive materials outlined in Ref. [7]. These properties

were leveraged to demonstrate excellent broadband sound barriers [9], broadband nonreciprocal media [10–13], and programmable extreme anomalous reflectors [14].

These exciting applications stem from the nonconventional wave equation governing the propagation of sound in Willis media. However, the exotic form of this equation, which was also associated to moving media [15–17], has been an impediment for our understanding of Willis media dynamics because there are no generally accepted solvers of this equation. Analytical solutions have been provided in one-dimensional (1D) systems [3,11,18] and in related homogeneous unbounded media [19], but these approaches are not suitable for two-(2D) or three-dimensional (3D) spaces involving finite-sized inhomogeneous materials.

In an attempt to overcome this obstacle, researchers resorted to equivalent models that equate Willis media with arrangements of discrete, line- or pointlike sources [9,10,20,21] separated by subwavelength distances. These models necessarily consider the microscopic interaction between these sources and are nonscalable in general scenarios in which the material they model becomes too voluminous. Moreover, it is generally challenging to relate the physical structure of a material to the strength of these sources [21].

In this work we address these challenges and derive the equivalence between general inhomogeneous Willis media anisotropic in both the mass density and Willis coupling vectors and conventional media with embedded continuous source distributions. The advantage of our approach is threefold. First, the latter medium is acoustically described by a wave equation which assumes a conventional form and thus can be solved numerically with commercially available solvers such as COMSOL Multiphysics. Consequently, our

*udemir@umich.edu
†bipopa@umich.edu

model enables efficient simulations of sound scattering from Willis media of arbitrary shape and material parameters in 2D and 3D. Second, this work gives previously unavailable insights into the physics of Willis materials. For example, it shows that multiple choices of Willis coupling vectors yield the same sound scattering characteristics in active Willis media. Third, our model answers important questions related to Willis material design such as whether the material parameters observed in single cell measurements extend to larger metamaterial samples obtained by periodically replicating that cell. We validate this equivalence model by showing that the sound scattered by a physical Willis metamaterial composed of unit cells of known effective material parameters matches excellently the field scattered by its continuous equivalent medium. We show that, remarkably, this excellent match occurs not only outside the Willis metamaterial but also inside it. This equivalence model will open the path towards better understanding the interaction of sound and Willis materials and will facilitate the extension of established metamaterial design and characterization tools including those based on advanced machine learning techniques [22–24] to Willis media.

Equivalence model. Willis acoustic media in 3D are characterized by four effective material parameters, namely the mass density $\bar{\bar{\rho}}$, the bulk modulus B, the velocity to pressure $\vec{S}$, and the volumetric strain to momentum density $\vec{D}$ coupling terms. To preserve generality, these material parameters are allowed to vary with position to account for inhomogeneous Willis media. For passive materials $\vec{S} = \vec{D}$. However, given the emergence of active Willis materials, we relax this constraint and allow $\vec{S}$ and $\vec{D}$ to be different in this work. The constitutive equations in these general fluids are [20]

$$\vec{\mu} = \bar{\bar{\rho}} \cdot \vec{v} + \vec{D}\varepsilon,$$
$$-p = B\varepsilon + \vec{S} \cdot \vec{v}, \qquad (1)$$

where p is the acoustic pressure, $\vec{v}$ is the particle velocity, ϵ is the volumetric strain, and $\vec{\mu}$ is the linear momentum density. These equations are coupled with the following conservation of momentum and mass equations written in the harmonic regime using the $e^{j\omega t}$ time-variation convention:

$$-\nabla p = j\omega\vec{\mu},$$
$$j\omega\varepsilon = \nabla \cdot \vec{v}. \qquad (2)$$

Understanding how sound propagates in inhomogeneous media described by Eqs. (1) and (2) requires solving them numerically. However, the unconventional form of these equations due to the additional terms containing $\vec{S}$ and $\vec{D}$ means that established solvers are not suitable and developing new ones are not trivial.

We show in this section that we can always replace the Willis medium with an equivalent conventional fluid with embedded continuous distributions of monopole and dipole sources of same shape and size as the Willis medium, as illustrated in Fig. 1. Our goal is to derive the material properties of the equivalent fluid (namely, mass density tensor $\bar{\bar{\rho}}'$ and bulk modulus B') and the monopole Q_m and dipole $\vec{q}_d$ source terms such that the scattered pressure fields are the same for both materials regardless of excitation. The conventional wave equation in the equivalent medium assumes the form of the
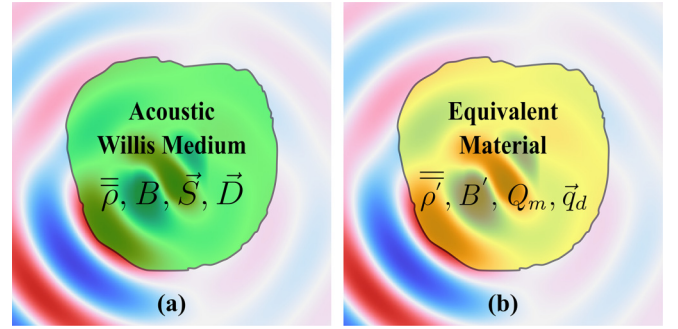

FIG. 1. Schematic diagrams of a general acoustic Willis medium with effective material parameters $\bar{\bar{\rho}}$, B, $\vec{S}$, and $\vec{D}$ and the acoustically equivalent continuous material with effective material parameters $\bar{\bar{\rho}}'$ and B' and embedded sources Q_m and $\vec{q}_d$.

inhomogeneous Helmholtz equation as follows [25]:

$$-\nabla \cdot [\bar{\bar{\rho}}'^{-1} \cdot (\nabla p - \vec{q}_d)] - \frac{\omega^2}{B'}p = Q_m. \qquad (3)$$

Similar to other source-driven models [9,20,26], the source terms Q_m and $\vec{q}_d$ are functions of the material parameters $\bar{\bar{\rho}}'$ and B', the local acoustic pressure p, and the pressure gradient ∇p. In the remainder of this section, we show that Eqs. (1) and (2) reduce to Eq. (3) under suitable choices of $\bar{\bar{\rho}}'$, B', Q_m, and $\vec{q}_d$ expressed in terms of $\bar{\bar{\rho}}$, B, $\vec{S}$, $\vec{D}$, p, and $\vec{v}$.

Substituting Eqs. (2) into Eqs. (1) yields

$$-\frac{1}{j\omega}\nabla p = \bar{\bar{\rho}} \cdot \vec{v} + \frac{\vec{D}}{j\omega}\nabla \cdot \vec{v}, \qquad (4)$$

and

$$-p = \frac{1}{j\omega}B\nabla \cdot \vec{v} + \vec{S} \cdot \vec{v}. \qquad (5)$$

From Eq. (4), $\vec{v}$ can be found in terms of the gradient of p and the divergence of $\vec{v}$ as follows:

$$\vec{v} = -\frac{1}{j\omega}\bar{\bar{\rho}}^{-1} \cdot (\nabla p + \vec{D}\nabla \cdot \vec{v}). \qquad (6)$$

Plugging $\vec{v}$ found above into the $\vec{S} \cdot \vec{v}$ term of Eq. (5) and rearranging the terms give

$$j\omega p = (M - B)\nabla \cdot \vec{v} + N, \qquad (7)$$

where

$$M = \vec{S} \cdot (\bar{\bar{\rho}}^{-1} \cdot \vec{D}),$$
$$N = \vec{S} \cdot (\bar{\bar{\rho}}^{-1} \cdot \nabla p), \qquad (8)$$

which gives the divergence of the particle velocity in terms of the acoustic pressure as follows:

$$\nabla \cdot \vec{v} = \frac{j\omega p - N}{M - B}. \qquad (9)$$

Computing the divergence of Eq. (6) and replacing $\nabla \cdot \vec{v}$ in it with the expression provided by Eq. (9) result in the wave equation in a Willis fluid written in terms of the acoustic pressure

$$\frac{j\omega p - N}{M - B} = -\frac{1}{j\omega}\nabla \cdot \left[\bar{\bar{\rho}}^{-1} \cdot \left(\nabla p - \vec{D}\frac{j\omega p - N}{B - M}\right)\right]. \qquad (10)$$

We notice that Eq. (10) is identical to the standard wave equation [Eq. (3)] in a conventional fluid with continuous distributions of monopole and dipole sources if and only if

$$\bar{\bar{\rho}}' = \bar{\bar{\rho}},$$

$$B' = B,$$

$$Q_m = j\omega B^{-1}\frac{N - j\omega p B^{-1}M}{1 - B^{-1}M},$$

$$\vec{q}_d = B^{-1}\vec{D}\frac{j\omega p - N}{1 - B^{-1}M}. \tag{11}$$

This is a remarkable result for at least three reasons. First, it shows that the Willis coupling terms in a general acoustic Willis medium could be simply replaced by distributions of monopole and dipole sources without modifying the acoustic pressure distribution inside and outside the medium. Therefore, instead of solving the nonconventional system of equations Eq. (1) and Eq. (2), one can simply solve the wave equation in the conventional equivalent material with embedded sources using commercial tools such as COMSOL Multiphysics.

Second, Eq. (11) provides important insights into the physics of Willis materials. One example regards the unicity of the Willis coupling terms producing a given acoustic field distribution. We note that in an active Willis material (which is not bound by the requirement $\vec{S} = \vec{D}$ existing in passive materials) there are in general six Willis vector components for $\vec{S}$ and $\vec{D}$ which could be used to manipulate the scattering of sound. Since the equivalent fluid with embedded sources has only four components that define the monopole and dipole sources that replace the effects of $\vec{S}$ and $\vec{D}$, it follows that there are multiple choices of $\vec{S}$ and $\vec{D}$ that result in the same scattered field distribution. This is better seen by noticing that the Willis vector $\vec{S}$ appears in the wave equation Eq. (10) as part of the definitions of scalars M and N in Eq. (8). For given values of M, N, $\bar{\bar{\rho}}$, $\vec{D}$, and p, Eq. (8) forms a system of two equations in the three unknowns comprising the components of vector $\vec{S}$. This is an underdetermined system having, in general, multiple solutions. Other insights into the physics of Willis metamaterials will be revealed after we consider the validation of Eq. (11) in the next section.

Third, models of matter consisting of conventional fluids with embedded sources have been shown to provide design tools for active metamaterials composed of periodic arrangements of sensors and drivers which realize the monopole and dipole sources in a straight-forward manner [26,27]. This model extends the same benefits to active Willis metamaterials. It provides the closed-form relationship between the local acoustic fields and the embedded source strengths. The relationship translates directly into the transfer functions between the sensors that capture the local acoustic fields and the actuators that produce the acoustic response in active metamaterials realized with the sensor-driver architecture.

Model validation. We validate next the equivalence model represented by Eqs. (11) by showing that it accurately calculates the sound scattered by a finite metamaterial sample composed of periodic arrangements of unit cells with known effective material parameters. This is done by showing that the scattered pressure fields from the physical metamaterial
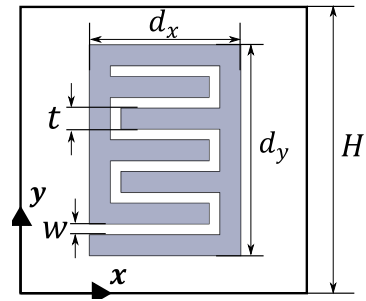

FIG. 2. Schematic diagram of the unit cell with $H = 11$ mm, $d_x = 5.75$ mm, $d_y = 8.00$ mm, $t = 0.8$ mm and $w = 0.4$ mm. The grey region is the rigid solid inclusion, and the white region is the background lossless air with density $\rho_0 = 1.29$ kg/m^3 and speed of sound $c_0 = 343$ m/s.

match very well those of the equivalent continuous material with embedded sources. To facilitate numerical simulations of a physical Willis metamaterial stucture composed of one-hundred-unit cells, we perform this validation in 2D.

The unit cells that make up the physical metamaterial are designed to be asymmetrical structures to induce anisotropy in the Willis coupling vectors and the mass density tensor. There are many approaches to realize acoustic Willis metamaterials [5,6,18,28,29]. Here we choose the typical labyrinthine design shown in Fig. 2, which was shown to lead to large Willis coupling terms [7]. In the figure, the grey region is the solid inclusion, and the white region is the background lossless air with density $\rho_0 = 1.29$ kg/m^3 and speed of sound $c_0 = 343$ m/s. The solid inclusion is assumed to be orders of magnitude stiffer and denser than air and thus its surface is well approximated by a perfect reflector.

The unit cell has the side lengths H, and the solid inclusion has the side lengths d_x and d_y, the wall thickness t, and the channel width w. These values were chosen using the following design procedure. It is common to consider that physical metamaterials formed by periodic arrangements of unit cells have effective material parameters if these unit cells are highly subwavelength structures [30]. As a rule of thumb, unit cell sizes smaller than a fifth of the wavelength in both the material and the background fluid usually suffice. Here we targeted the 2−4 kHz bandwidth corresponding to wavelengths in air (λ_0) between 85.75 mm and 171.5 mm. We thus choose the unit cell size $H = 11$ mm, which is approximately one-tenth of $\lambda_0 = 114.3$ mm at 3.00 kHz. The meandered path length was chosen to be approximately a quarter of the wavelength at 3 kHz to produce significant Willis parameters at this frequency. The inlet position was chosen on the bottom left side of the cell to ensure Willis anisotropy in the $\vec{S} = \vec{D}$ vectors, i.e., $0 \neq S_x \neq S_y \neq 0$, where S_x and S_y are the components of these vectors in the x and y directions.

The mass anisotropy of the cell is determined by the asymmetry in the inclusion dimensions. To assure large differences between the mass density tensor components in the principal axes ρ_{xx} and ρ_{yy}, we chose d_x significantly smaller than d_y.

The other geometrical parameters were chosen iteratively by requiring large mass density and Willis parameter anisotropies in the metamaterial. For each choice of geometrical parameters, the effective $\bar{\bar{\rho}}$, $\vec{S}$, and $\vec{D}$ were calculated
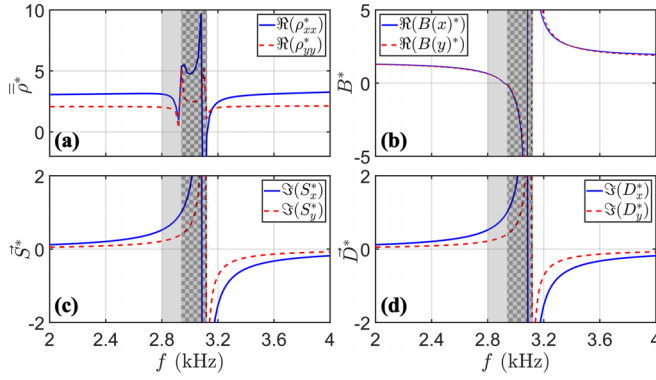
FIG. 3. Nondimensional effective material parameters extracted from 1D unit cell simulations: (a) $\Re(\rho_{xx}^*)$ and $\Re(\rho_{yy}^*)$, (b) $\Re(B^*)$, (c) $\Im(S_x^*)$ and $\Im(S_y^*)$, and (d) $\Im(D_x^*)$ and $\Im(D_y^*)$.

from sound reflection and transmission simulations through one unit cell in a 1D setting using an established procedure [10,11,31]. The components of these effective material parameter tensors were computed considering propagation in the x and y directions as described in [32]. Furthermore, although being a scalar term, B was also obtained independently from sound propagation in the x and y directions to confirm that they have very similar values for both directions.

The final geometrical design parameters are $d_x = 5.75$ mm, $d_y = 8.00$ mm, $t = 0.8$ mm and $w = 0.4$ mm, the length of the meandering paths is 29.7 mm, approximately one-quarter of $\lambda_0 = 114.3$ mm at this frequency. Figure 3 shows the extracted relative effective material parameters for this cell defined as $\bar{\bar{\rho}}^* = \bar{\bar{\rho}}/\rho_0$, $B^* = B/B_0$, $\vec{S}^* = \vec{S}/Z_0$, and $\vec{D}^* = \vec{D}/Z_0$ where $\rho_0 = 1.29$ kg/m^3, $B_0 = 0.152$ MPa and $Z_0 = 442.5$ Pa s/m are the mass density, bulk modulus, and characteristic impedance of air. In the frequency range 2.80–3.12 kHz, the cell size is larger than a fifth of the wavelength in the metamaterial, the homogenization theory becomes less accurate, and thus the effective material parameters lose physical meaning. In this band, the metamaterial displays phononic crystal characteristics showing either high dispersion (light gray area in Fig. 3) or a band gap (textured gray in the figure). Here we are primarily interested in the frequencies outside of this band where the homogenization theory is accurate. By doing so, we also disregard the nonlocal components of the Willis coupling terms, which make these coupling terms vary with impinging wave direction, as discussed in Ref. [33].

Owing to the constitutive equations defined in Eq. (1), the unit cell simulations reveal that for lossless Willis media, $\bar{\bar{\rho}}^*$ and B^* are real for all propagating frequencies and that $\vec{S}^*$ and $\vec{D}^*$ are purely imaginary. Therefore, Fig. 3 shows the real values of mass density $\Re(\bar{\bar{\rho}}^*)$ and bulk modulus $\Re(B^*)$, and the imaginary values of Willis coupling vectors $\Im(\vec{S}^*)$ and $\Im(\vec{D}^*)$ over the frequency range 2–4 kHz. The imaginary parts of $\vec{S}^*$ and $\vec{D}^*$ may mean that the impulse momentum depends on the rate of change of the volumetric strain and the acoustic pressure depends on the particle acceleration, as discussed in Ref. [18]. In this case, the Willis coupling terms $\vec{S}$ and $\vec{D}$ would be replaced by $j\omega\vec{S}$ and $j\omega\vec{D}$ in the constitutive
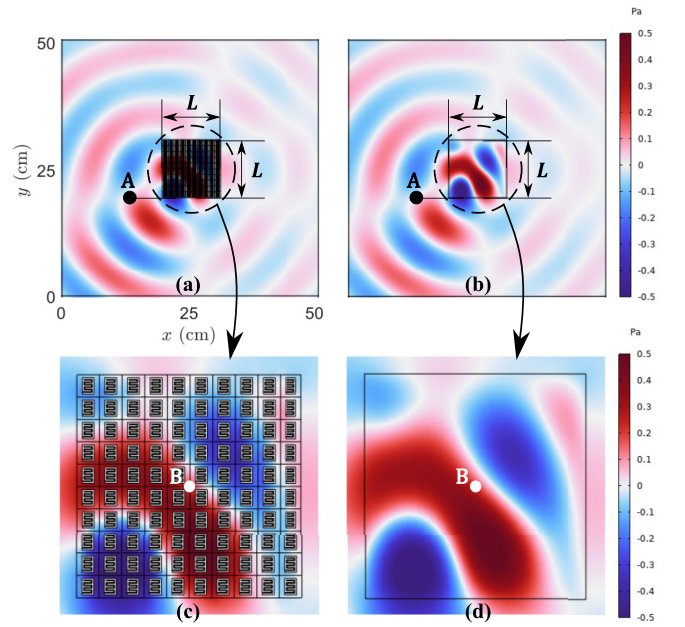

FIG. 4. Scattered pressure fields from (a) the Willis medium and (b) the acoustically equivalent continuous material with embedded sources at $f = 2.80$ kHz. Close-up views of the scattered pressure fields inside (c) the Willis medium and (d) equivalent material. The plots present the raw fields computed by COMSOL Multiphysics.

Eqs. (1) and, therefore, the redefined Willis coupling terms become real. In this work, we chose the form of the constitutive equations shown in Eqs. (1) as this form is more widely used.

Figure 3 confirms that the unit cell has significant anisotropy in the mass density [Fig. 3(a)] and Willis coupling vectors [Figs. 3(c) and 3(d)]. The extracted bulk modulus [Fig. 3(b)] assumes the same values outside of the shaded regions, which confirms the metamaterial behaves acoustically as a fluid. Finally, as expected for passive lossless media, it is seen that $\vec{S} = \vec{D}$.

Having designed a Willis unit cell with known effective material parameters, we validate our equivalence model for Willis media by comparing the acoustic fields scattered by a metamaterial composed of periodic arrangements of this unit cell and its equivalent continuous fluid with embedded sources and acoustic properties provided by Eq. (11).

The metamaterial is the 10 by 10 lattice of unit cells shown in Fig. 4(a) such that it forms a square with side $L = 110$ mm or almost a wavelength in air. The metamaterial was ensonified by a line source placed at the coordinate $(x, y) = (576, 576)$ mm and of frequency 2.8 kHz (i.e., the frequency just to the left of the left shaded region in Fig. 3). The complex acoustic pressure distribution scattered by the physical metamaterial is shown in Fig. 4(a).

The effective material parameters at this frequency are obtained from Fig. 3 and assume the following values: $\Re(\rho_{xx}^*) = 3.06$ and $\Re(\rho_{yy}^*) = 2.02$, $\Re(B^*) = 0.65$, $\Im(S_x^*) = \Im(D_x^*) = 0.52$, and $\Im(S_y^*) = \Im(D_y^*) = 0.22$. These values were plugged into Eqs. (11) to calculate the effective properties of the equivalent continuous material with embedded sources. The acoustic pressure scattered by this equivalent material is shown in Fig. 4(b).
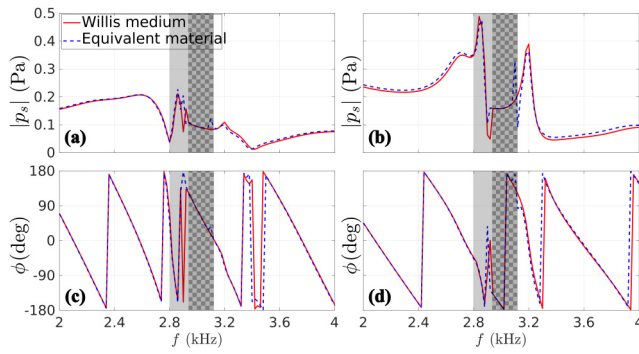
FIG. 5. The scattered pressure magnitudes at (a) point A and (b) point B and the scattered pressure phases at (c) point A and (d) point B for the Willis metamaterials (solid line) and the equivalent material (dashed line).

It can be seen from Figs. 4(a) and 4(b) that the pressure fields scattered from the equivalent continuous material are in excellent agreement with those scattered from the physical Willis metamaterial. More importantly, the close-up views of the pressure fields obtained inside the Willis metamaterial match equally well those in the equivalent medium as illustrated in Figs. 4(c) and 4(d). These results confirm the effectiveness of the equivalence model summarized by Eq. (11).

To further validate this model, we performed this comparison in the entire band from 2 kHz to 4 kHz and recorded the acoustic pressure amplitude and phase at two points inside and outside the metamaterial labeled A and B in Fig. 4. The magnitude $|p_s|$ and phase ϕ of the scattered pressure fields for the Willis media and its equivalent continuous material counterpart are shown in Figs. 5(a) and 5(c) for point A and Figs. 5(b) and 5(d) for point B. The simulations inside the continuous material match very well the fields obtained in the Willis metamaterial over the entire frequency range with the exception of a few regions discussed below where some discrepancies occur.

For point A, there is a mismatch in the phase values for $3.39 \leqslant f \leqslant 3.42$ kHz [Fig. 5(c)]. This is expected because the pressure field amplitudes approach zero and thus the phase values lose relevance. Moreover, for point B, the equivalent material shows spikes in the scattered pressure amplitude $|p_s|$ and phase ϕ in a narrow band around $f = 3.10$ kHz where the bulk modulus B approaches the term M given by Eqs. (8) and jωp approaches N to maintain a finite value of the source terms Q_m and $\vec{q}_d$. At these frequencies, Eq. (11) becomes very sensitive to numerical errors in the computation of the acoustic pressure. As mentioned before, the effective material parameters shown in Fig. 3 lose physical meaning in the gray band shown in Fig. 3 (2.80–2.94 kHz) where the metamaterial display phononic crystal characteristics. Nevertheless, it is remarkable to see that the good match between the fields scattered by the physical metamaterial and its equivalent model in this band. This observation suggests that, for this specific metamaterial, the homogenization theory holds for cell sizes significantly larger than a fifth of the wavelength inside the metamaterial.

We further validate our equivalent medium model by computing the average rate of change of energy inside the medium over a period and showing it is zero for the lossless metamaterial. According to the conservation of energy, the average rate of change of energy can be computed by integrating the acoustic intensity vector $\vec{I} = 0.5\Re(p\vec{v}^*)$ over a closed surface surrounding the effective medium. The details of this calculation, the estimated acoustic intensity vector, and the rate of change of energy relative to the power incident are presented in the Supplemental Material [34] (see also Ref. [35] therein). This calculation shows that the energy rate of change is negligible compared to the impinging power in the entire band of interest where the homogenization theory holds, i.e., excluding the gray region in Fig. 3. This confirms once more the validity of our equivalent medium model.

The excellent match between the simulated acoustic pressure for the Willis metamaterial and its equivalent continuous counterpart demonstrates directly that the effective material parameters retrieved from one-cell simulations maintain validity in the bulk metamaterial composed of large numbers of cells. This remarkable result confirms that the acoustic behavior of the labyrinthine Willis cell shown in Fig. 2 is not influenced by the other cells surrounding it. This result is not surprising. The Willis coupling terms are expected to be influenced by the length and shape of the meandered channel inside the solid inclusion rather than by external factors. Also, metamaterials made of solid nonresonant rectangular inclusions were shown to have the same effective acoustic properties as the individual cell spawning it [32]. For example, it was shown that the extracted effective material properties of such a nonresonant metamaterial varying in thickness from 1 to 4 unit cells along the propagation direction are essentially the same in the frequency band where the unit cell size is significantly smaller than the wavelength [32]. This observation implies that the behavior of individual cells remains uninfluenced by interactions between them. However, this important property may not hold for other metamaterial cells. For example, it was shown that cells based on Helmholtz resonators [36] possess distinct effective material properties compared, depending on whether the cells are placed at the edge or in the middle of the metamaterial. In this case, imparting the effective properties extracted from a single cell to a bulk metamaterial yields significant errors. Importantly, the equivalence model and the validation method presented in this work constitute a straight-forward procedure to obtain insight into when one-cell effective properties extend to bulk metamaterials.

Conclusion. In this study, we derived the wave equation in a general inhomogeneous, anisotropic acoustic Willis medium and showed that it is identical to the wave equation in a conventional fluid with continuous distributions of monopole and dipole sources. To maintain maximum generality, the derivation did not make assumptions about the relationship between the Willis coupling vectors and thus is applicable to both passive and active media. This result shows that the physics of Willis materials can be efficiently analyzed by studying its equivalent conventional fluid for which efficient solvers of the wave equation exist in 1D, 2D, and 3D. This approach was validated through the excellent match between the acoustic pressure scattered by a physical Willis metamaterial and its continuous equivalent. This equivalence gave insights into the

physics of acoustic Willis media. For example, it showed that there exist multiple pairs of Willis coupling vectors that can produce identical sound scattering, but these Willis coupling terms are typically characteristic of the active media. Moreover, the equivalence also demonstrated directly that the bulk metamaterials obtained by periodic arrangements of a popular type of anisotropic labyrinthine unit cell of known effective material parameters maintain the effective acoustic properties of the cell. This implies that single cell design is a very effective tool for the design of large metamaterials involving this type of cell.

Due to its ability to efficiently perform simulations of sound scattered by acoustic Willis materials, the approach will allow researchers to apply advanced methods developed for conventional media (e.g., based on machine learning) to design and characterize Willis media.

[1] J. R. Willis, Variational principles for dynamic problems for inhomogeneous elastic media, Wave Motion **3**, 1 (1981).

[2] G. W. Milton and J. R. Willis, On modifications of newton's second law and linear continuum elastodynamics, Proc.: Math. Phys. Eng. Sci. **463**, 855 (2007).

[3] J. R. Willis, Exact effective relations for dynamics of a laminated body, Mech. Mater. **41**, 385 (2009).

[4] J. R. Willis, Effective constitutive relations for waves in composites and metamaterials, Proc.: Math. Phys. Eng. Sci. **467**, 1865 (2011).

[5] S. Koo, C. Cho, J.-h. Jeong, and N. Park, Acoustic omni meta-atom for decoupled access to all octants of a wave parameter space, Nat. Commun. **7**, 13012 (2016).

[6] J. Li, C. Shen, A. Díaz-Rubio, S. A. Tretyakov, and S. A. Cummer, Systematic design and experimental demonstration of bianisotropic metasurfaces for scattering-free manipulation of acoustic wavefronts, Nat. Commun. **9**, 1342 (2018).

[7] L. Quan, Y. Ra'di, D. L. Sounas, and A. Alù, Maximum Willis coupling in acoustic scatterers, Phys. Rev. Lett. **120**, 254301 (2018).

[8] J. Li, A. Song, and S. A. Cummer, Bianisotropic acoustic metasurface for surface-wave-enhanced wavefront transformation, Phys. Rev. Appl. **14**, 044012 (2020).

[9] B.-I. Popa, Y. Zhai, and H.-S. Kwon, Broadband sound barriers with bianisotropic metasurfaces, Nat. Commun. **9**, 5299 (2018).

[10] Y. Zhai, H.-S. Kwon, and B.-I. Popa, Active Willis metamaterials for ultracompact nonreciprocal linear acoustic devices, Phys. Rev. B **99**, 220301(R) (2019).

[11] N. Geib, A. Sasmal, Z. Wang, Y. Zhai, B.-I. Popa, and K. Grosh, Tunable nonlocal purely active nonreciprocal acoustic media, Phys. Rev. B **103**, 165427 (2021).

[12] C. Cho, X. Wen, N. Park, and J. Li, Acoustic Willis meta-atom beyond the bounds of passivity and reciprocity, Commun. Phys. **4**, 82 (2021).

[13] S. R. Craig, B. Wang, X. Su, D. Banerjee, P. J. Welch, M. C. Yip, Y. Hu, and C. Shi, Extreme material parameters accessible by active acoustic metamaterials with Willis coupling, J. Acoust. Soc. Am. **151**, 1722 (2022).

[14] Y. Zhai, H.-S. Kwon, and B.-I. Popa, Anomalous reflection with omnidirectional active metasurfaces operating in free space, Phys. Rev. Appl. **16**, 034023 (2021).

[15] H. Nassar, X. Xu, A. Norris, and G. Huang, Modulated phononic crystals: Non-reciprocal wave propagation and Willis materials, J. Mech. Phys. Solids **101**, 10 (2017).

[16] L. Quan, D. L. Sounas, and A. Alù, Nonreciprocal Willis coupling in zero-index moving media, Phys. Rev. Lett. **123**, 064301 (2019).

[17] L. Quan, S. Yves, Y. Peng, H. Esfahlani, and A. Alù, Odd Willis coupling induced by broken time-reversal symmetry, Nat. Commun. **12**, 2615 (2021).

[18] M. B. Muhlestein, C. F. Sieck, A. Alù, and M. R. Haberman, Reciprocity, passivity and causality in Willis materials, Proc.: Math. Phys. Eng. Sci. **472**, 20160604 (2016).

[19] Y.-G. Peng, Y. Mazor, and A. Alù, Fundamentals of acoustic Willis media, Wave Motion **112**, 102930 (2022).

[20] C. F. Sieck, A. Alù, and M. R. Haberman, Origins of Willis coupling and acoustic bianisotropy in acoustic metamaterials through source-driven homogenization, Phys. Rev. B **96**, 104303 (2017).

[21] H. Esfahlani, Y. Mazor, and A. Alù, Homogenization and design of acoustic Willis metasurfaces, Phys. Rev. B **103**, 054306 (2021).

[22] Y. Zhai, H.-S. Kwon, Y. Choi, D. Kovacevich, and B.-I. Popa, Learning the dynamics of metamaterials from diffracted waves with convolutional neural networks, Commun. Mater. **3**, 53 (2022).

[23] Y. Cheong, H.-S. Kwon, and B.-I. Popa, Metamaterial characterization from far-field acoustic wave measurements using convolutional neural network, Front. Phys. **10**, 1021887 (2022).

[24] W. Zhou, S. Wang, Q. Wu, X. Xu, X. Huang, G. Huang, Y. Liu, and Z. Fan, An inverse design paradigm of multi-functional elastic metasurface via data-driven machine learning, Mater. Des. **226**, 111560 (2023).

[25] A. D. Pierce and R. T. Beyer, *Acoustics: An Introduction to its Physical Principles and Applications, 1989 Edition* (ASA, Melville, NY, 1990).

[26] D. A. Kovacevich and B.-I. Popa, Transformation acoustics with bulk media composed of polarized sources, Phys. Rev. B **104**, 134304 (2021).

[27] D. A. Kovacevich and B.-I. Popa, Programmable bulk modulus in acoustic metamaterials composed of strongly interacting active cells, Appl. Phys. Lett. **121**, 101701 (2022).

[28] A. Merkel, V. Romero-García, J.-P. Groby, J. Li, and J. Christensen, Unidirectional zero sonic reflection in passive pt-symmetric Willis media, Phys. Rev. B **98**, 201102(R) (2018).

[29] A. Melnikov, Y. K. Chiang, L. Quan, S. Oberst, A. Alù, S. Marburg, and D. Powell, Acoustic meta-atom with experimentally verified maximum Willis coupling, Nat. Commun. **10**, 3148 (2019).

[30] Y. Xie, B.-I. Popa, L. Zigoneanu, and S. A. Cummer, Measurement of a broadband negative index with space-coiling acoustic metamaterials, Phys. Rev. Lett. **110**, 175501 (2013).

[31] M. B. Muhlestein, C. F. Sieck, P. S. Wilson, and M. R. Haberman, Experimental evidence of Willis coupling in a one-dimensional effective material element, Nat. Commun. **8**, 15625 (2017).

[32] B.-I. Popa and S. A. Cummer, Design and characterization of broadband acoustic composite metamaterials, Phys. Rev. B **80**, 174303 (2009).

[33] M. Malléjac, T. Cavalieri, V. Romero-García, A. Merkel, D. Torrent, J. Christensen, J. Li, and J.-P. Groby, Non-locality of the willis coupling in fluid laminates, Wave Motion **110**, 102892 (2022).

[34] See Supplemental Material at http://link.aps.org/supplemental/10.1103/PhysRevB.109.L020301 for computing the acoustic power through a surface enclosing the equivalent medium, which includes Ref. [35].

[35] L. E. Kinsler, A. R. Frey, A. B. Coppens, and J. V. Sanders, *Fundamentals of Acoustics*, 4th ed. (John Wiley & Sons, Hoboken, NJ, 2000).

[36] J. Morris and A. V. Amirkhizi, Multi-point scattering measurements for effective property extraction from metamaterials with skin effects, Int. J. Solids Struct. **279**, 112372 (2023).